VERIZONA PUBLISHER
Publishing Your Ideas

www.verizonaonlinepublishing.com
Vol: 1, Issue: 3

Journal of Nanoscience with Advanced Technology

Nanoengineering of Hybrid Lightweight Cellulosic Fibre Foams for better Flame Resistance

Carl Lange[1*], Jan Erik Eriksson[2], Jani Lehmonen[3], Marjukka Tuominen[4], Paul Ek[5] and Pedro Fardim[1,6*]

[1] Åbo Akademi University, Faculty of Science and Engineering, Laboratory of Fibre and Cellulose Technology, Porthansgatan 3-5, FI-20500, Åbo FINLAND

[2] Åbo Akademi University, Faculty of Science and Engineering, Laboratory of Inorganic Chemistry, Biskopsgatan 8, FI-20500, Åbo FINLAND

[3] VTT Technical Research Centre of Finland Ltd., Jyväskylä, Finland

[4] University of Turku, Department of Physics and Astronomy, Materials Research Laboratory, Vesilinnantie 5, FI-20014, Turku FINLAND

[5] Åbo Akademi University, Faculty of Science and Engineering, Laboratory of Analytical Chemistry, Biskopsgatan 8, FI-20500, Åbo FINLAND

[6] KU Leuven, Department of Chemical Engineering, Celestijnenlaan 200F bus 2424, B-3001 Leuven, Belgium

***Corresponding author:** Pedro Fardim, KU Leuven, Department of Chemical Engineering, Celestijnenlaan 200F bus 2424, B-3001 Leuven, Belgium; Email: pfardim@abo.fi

Carl Lange, Åbo Akademi University, Faculty of Science and Engineering, Laboratory of Fibre and Cellulose Technology, Porthansgatan 3-5, FI-20500, Åbo FINLAND; Email: clange@abo.fi

Article Type: Research, **Submission Date**: 03 November 2015, **Accepted Date:** 20 November 2015, **Published Date:** 11 December 2015.

Citation: Carl Lange, Jan Erik Eriksson, Jani Lehmonen, Marjukka Tuominen, Paul Ek, et al. (2015) Nanoengineering of Hybrid Lightweight Cellulosic Fibre Foams for better Flame Resistance. J Nanosci Adv Tech 1(3): 1-13.

Abstract

We studied the flame propagation and combustion properties of a lightweight fibrous foam produced from a layered double hydroxides (LDH) modified thermomechanical pulp fibres. The *in situ* synthesis of Mg-Al LDH with pulp fibres was engineered to include both micron and nano-sized particles. The method allowed loading the fibres with LDH up to 34% (w/w). Observed pyrolytic effects included 60% reduction in CO_2 production rate, and similar reductions in peak heat release rate (PHRR) and in amount of soot during the oxidative pyrolysis. The *in situ* synthesised LDH particles shielded the fibres from external heat by reducing the rate of oxidation and liberation of volatile gases. Effective charring was observed at the interphase of LDH nanoparticles and organic material.

Keywords: Cone calorimeter, ESCA, Flame retardant, LDH, Light weight foam, Softwood, Spruce, XPS.

Introduction

Mass production of foam-laid fibrous material was initiated in the pulp and paper industry in late '20s [1]. Soap was applied to wood pulp suspension was to create labile bubbles that aided fibre disintegration and formation of aerated suspension. The resulting material had significantly higher volume to mass ratio in comparison to wet-laid fibre suspensions and it bared softness and fluffiness comparable to cotton. Additives were also included in formulation and some of them, such as casein, imparted rigidity to the foamed structure and thus brought new application possibilities for pulp fibres reach. However, it took some 30 years before foaming process received further attention in the given field as researchers in late '50s begun to improve the uniformity, density and softness of the nonwoven products that were already in the market [2,3,4]. The practical challenges at the time were often associated with the fibre web formation and material strength [5,6]. It was soon noticed that the flexibility of the fibres, draining and dewatering of the foamed fibre web by pressing, and, the control of the foam structure during the web formation with a surfactant of choice were the most important factors affecting the desired properties in the final product.

While the progress in foam formation process has been stagnant in paper and packaging industry since '70s – after the advent of commercial polymeric and aluminium foams – utilization of natural fibres is not completely forgotten and the foam-laid system is appearing potential to resolve some of the industrially related problems that are encountered in the traditional wet-laid manufacturing [7,8]. For example, as modified cellulose materials were found to be challenging in conventional processes, particularly from the point of view of dewatering and web forming characteristics [9], the foam forming technology has offered an alternative in which different starting materials ranging from nanometres up to millimetres in length can be processed with high uniformity [10,11,12]. It has been noted that foam formation is especially advantageous in utilization of long fibres as they are known to form agglomerated structures from a wet-laid sludge. In addition, considering the environmental aspects, the amount of water in the production may be reduced with respect to typical wet-laid process. Furthermore, as pulp

industry is under a pressure to get more revenues from a smaller amount of raw material, the foam forming technology enables better bulk in the product while strength remains at sufficient level [7]. Also, the foam formation has advantage over the wet-laid system if cellulosic fibres are used in combination with the synthetic ones [13]. Some patents has also been filed relatively recently as opportunities in competition against the existing technologies have arisen in foam formation of fibrous materials [14,15]. The challenge that still remains and often inhibits further applicability of natural fibres regardless of the manufacturing method or material architecture – be they panels, laminates, multi-layered structures, beams, paper, board or light weight foams – however, is their tendency to absorb large amounts of water and ignite upon spark or flame.

Flame retardants are important additives in house hold materials, public transport interiors, in insulations, electrical devices, and so on. Applications that involve foamed structures from fibres or polymers are always subject to hazardous flame propagation or melting in case of fire. The initial liberation of volatile gases may spread the fire with considerable rate especially if material density is low. Advancing pyrolysis zone in low density material that does not contain flame retardants cannot prevent the heat flux of burning gases to suddenly liberate even more volatiles from a large surface area that eventually incinerates the material. Most common industrial scale flame retardants are based on polyhalogenated compounds and polyphosphates [16] and also on inorganic particles mainly magnesium and aluminium hydroxides. Alternatives are sought as the health related issues in context of halogenated and phosphorous flame retardants prohibits industries to apply them in the future [17]. Even still, these chemicals and the items that contain them have a long life span and people will continue to be exposed to their adverse effects for a number of years. The mode of action of halogenated flame retardants is in their ability to form free radicals that ultimately react with the polymer or the volatile components in the gas phase before they reach ignition temperature. Thus they facilitate effective heat reduction and charring that prevents fuelling the fire. Phosphorous compounds react in pyrolytic process through polymerization that effectively serves as a barrier against the heat and liberation of volatiles in the solid phase. Benefits from the inorganic particles, particularly $Mg(OH)_2$ and $Al(OH)_3$, as flame retardants come in the form of released water vapour, endothermic decomposition and char formation. A disadvantage of inorganic particulate flame retardants is associated in their inefficiency in comparison to halogenated and phosphorous compounds. High loadings of inorganic particles are usually required, which tend to alter the material's physical properties.

Hydrotalcite is a layered solid comprised from two dimensional magnesium-aluminium hydroxides sheets that have intercalated carbonate anion in between them. Thermal decomposition behaviour of hydrotalcite and its analogues, generally named as layered double hydroxides (LDH), has been well documented [18,19,20]. Different LDH structures such as the ones where the intercalated species are interchanged to organic moieties, or, the divalent and trivalent cationic precursors and their fractional compositions being altered, have been evaluated as flame retardants in PVC, PS, ABS, PMMA and epoxy matrix among others [21-24]. The combustion energy is used up by LDH in several concomitant processes. These include: heat adsorption via water evaporation and crystalline phase transformations, gas dilution by liberated carbon dioxide and water, smoke suppression by adsorption of volatile components, and, char formation. Besides these beneficial properties, only couple of reports, that we have found, relate the LDH material as a flame retardant in textile or paper products that use natural fibres [25,26]. As already mentioned, a large amount of inorganic particles is typically required to attain sufficient reduction in flammability. LDH have a particularly interesting property that neither of the constituent precursors, $Mg(OH)_2$ or $Al(OH)_3$, has in themselves. LDH carry a net positive charge due to trivalent aluminium. To counter that charge build up there are intercalated anionic components in between its lamella. These anions can be chosen rather freely. Pulp fibres are naturally acidic facilitating electrostatic interaction with LDH in neutral or alkaline medium. Therefore the synthesis of LDH *in situ* with pulp fibres may bring additional benefit to the foam-laid process in which the addition of flame retardants after the foam has been formed is difficult unless it is inherently part of the matrix.

In this article we address the flammability and burning behaviour of nanoengineered lightweight fibrous foam (lwFF) that contains carbonate intercalated micron and nano-sized LDH (LDH-lwFF). These particles were synthesised *in situ* with pulp fibres prior to foam formation. We have studied the material flammability, elemental composition, combustion kinetics, particle distribution and size on fibre surfaces. Also, a high speed video recorder (HSvid) was coupled with a microscope to visualize the ignition and combustion phenomena.

Materials and Methods

The following chemicals and materials were used: $Mg(NO_3)_2{\cdot}6H_2O$ (98-102%, Sigma-Aldrich, UK), $Al(NO_3)_3{\cdot}9H_2O$ (≥ 98%, Sigma-Aldrich, Germany), urea ($CO(NH_2)_2$, ≥ 99.0-100.5%, Merck, Germany). Sodium dodecyl sulphate ($NaC_{12}H_{25}SO_4$, 98%, Sigma-Aldrich, Japan) was used in foam-laid formation. Hydrogen peroxide bleached thermomechanical pulp (BTMP) from spruce (*Picea Abies*) was received from UPM, Rauma Mill, Finland, and used in the foams.

Nanoengineering of fibres that contain LDH with intercalated carbonate anion was carried out *in situ* by sequenced urea hydrolysis and co-precipitation. A batch of 150g (oven dry weight) of BTMP was initially suspended in a beaker into 1000ml of distilled water. LDH precursors with urea were dissolved in 1000ml of distilled water in another beaker. The sludge and the solution were mixed and the fibres were allowed to soak for 60min at room temperature. Total metal ion concentration () in the pulp sludge was 375mM while the Mg and Al precursor ratio was 2:1. Urea was used in an amount corresponding to $10{\cdot}n_{Al}$ (1.249M). The sludge was then transferred into a preheated (93°C) 3000ml Teflon® lined reactor vessel that was fitted with a powerful wing rotor to assure efficient mass transport of ions and material mixing at relatively high consistency (7.5%). Due to material addition into the reactor, the sludge was allowed to heat up to 90°C in static conditions prior the initiation of mixing sequence (20rpm for 10 seconds in every three minutes). Total reaction time was 180 minutes. After the LDH synthesis, the sludge was divided into two 1000 ml reactor vessels for hydrothermal treatment at 130±10°C for 12 hours. Finally the pulp fibres were repetitiously washed by dispersing them into

5000ml cold distilled water using Büchner-funnel for filtration. Further dewatering of sludge was performed din a centrifuge to approximately 33% consistency before dispersing it into the next washing solution.

In the nanoengineering sequence the micron sized LDH containing pulp fibres were further modified via homogeneous co-precipitation of LDH particles by dispensing NaOH (1.0M) and the metal precursors (0.5M) from two titrators until the in the sludge reached 25mM concentration. The method is described in detail in our previous work [27]. The purpose for two separate treatment sequences was to mineralize the fibres via urea hydrolysis and synthesise nanoparticles onto the fibre surface in concomitant homogeneous co-precipitation.

Lightweight fibrous foam formation was carried out in the laboratory scale utilizing the special in house build foam-laid sheet former. The average grammage of formed structures were 100gm^{-2}. Tap water was used as process water and sodium dodecyl sulphate as the foaming agent. The procedure was as follows. At first, an aqueous fibre suspension was mixed with the prefabricated foam that was produced by vigorous stirring (3500rpm) of SDS containing water. The dosage of SDS was optimized to 0.15-0.2gL^{-1} leading to 60-70% air content in the foam. When the fibre foam state was stabilized, it was decanted into the hand sheet mould. A ten millimetre slit was positioned in between the plate end and the mould wall to restrict the spreading speed of foam to the wire, on which the foam ultimately formed, and also to force the foam to spread in one direction. This system provides shear forces that are high enough to orient the fibres with the direction of the flow. After the foam was settled in the mould, in the dewatering phase, it was filtered through the wire using a vacuum suction. The sheet was then detached from the mould with the transferring wire and pre-dried on a special suction table. The suction table was equipped with a 5mm wide slid that enabled air to pass through the foam-laid sheet at vacuum conditions corresponding to 0.2 bars.

Inductively coupled plasma mass spectrometer (ICP-MS), Perkin Elmer Sciex, Elan 6100 DRC Plus (Framingham, MA, USA) was used to quantify the Mg and Al in foam formed fibre samples. Fibres were previously dissolved with 5ml of nitric acid (supra pure) and 1ml of H_2O_2. The slurry was then heated inside of the microwave bombs made out of Teflon to 200°C with autogenous pressure build up to ensure a complete dissolution.

Thermogravimetric analysis (TGA) was performed with TA-Instrument's SDT Q600 (New Castle, DE, USA) under air atmosphere. An alumina sample pan (60µL) was used in all experiments and the specimens were pelletized with a custom made pelletizer to match 600±25 kgm^{-3} density. The gas flow rate was set to 100 ml min^{-1} and heating rate to 5°C min^{-1}. Temperature was ramped in between 25–525°C.

Infrared spectrophotometer (FTIR), Thermo Scientific, Nicolet iS50 FT IR (Madison, WI, USA) with attenuated total reflection setup was used in analysis of foam formed panels. Instrument was equipped with a diamond crystal and a pressure gauge. The pressure was set to 30±2 kg in all samples. Total of 64 scans was recorded and corrected with the Omnic spectral suite software (v. 9.2.41) that provided ambient background and ATR correction for 45° incident angle with 1 refraction assuming 1.50 refractive index for all samples.

A Leo Gemini 1530 field emission scanning electron microscope (SEM) with In-Lens detector (LEO Electron Microscopy Ltd., Oberkochen, Germany) was the method for characterization of the LDH particles and pulp fibres. The samples were adhered onto the SEM sample holder with a copper tape and coated with carbon in Temcarb TB500 sputter coater (Emscope Laboratories, Ashford, U.K.). Optimum accelerating voltage for SEI imaging was 15 kV. Electron diffraction spectra (EDS) were acquired with 20 kV. Calibration was performed with cobalt. Five data points were randomly chosen from each sample to assess the amounts of Mg, Al and S in them.

Transmission electron microscope (TEM), JEOL JEM-1400 Plus (JEOL, Tokyo, Japan), was operated at 120 kV acceleration voltage and used to image samples that were embedded in 45359 Fluka Epoxy Embedding Medium kit and thin sectioned with an ultramicrotome to 200 nm thickness.

Cone Calorimeter (CC), Fire Testing Technology, (West Sussex, UK) was used according to the ISO 5660 and ASTEM E 1354 standards and applied for combustion analysis of foamed fibre web panels. Installation included a 3-term (PID) temperature controller and three type K thermocouples. Sample weight accuracy for the instrument is 0.01 g. Spark ignition system (10 kV) was used in all experiments. Nominal duct flow rate was set to 24 L min^{-1}. The sample panels were cut to 94±2 mm squares with 7.5±0.5 mm in thickness and placed into aluminium trays (100±2 mm squares) for testing. The calculated flat surface area of all samples was 89±3 cm^2 and density 35±3 kgm^{-3}. The heat flux was set to 25kWm^{-2} and the surface of the specimen was positioned horizontally 60 mm below the heating element. Heater element and the sample were separated with a split shutter mechanism. Ambient conditions during the experiment were: T = 25°C, RH = 55% and p = 102.6kPa. Total of five samples were tested from two different batches.

High-Speed video recorder (HSvid) (Citius C 100 centurio, Citius Imaging Ltd, Finland) was set up to investigate the combustion process visually. The samples (approx. 8mm in diameter) were detached from the lwFF panels and placed on the top of a resistive wire (Alucrom I, Cr 20%, Al 5%, 42.200 Ω·m^{-1}). Also, an aluminium mesh was placed on top of the samples to maintain the focus throughout the video recording. A power supply (30W) was used for heating the resistive wire that ultimately burned the material. The high-speed camera was mounted to a tripod above the microscope camera ocular. The HSvid was equipped with 105 mm macro objective lens and the video was recorded through the microscope's objective lens using 10x magnification by taking an image on every 10ms interval at various ISO sensitivities (300–1080) and exposure times (0.5–2.0ms).

X-ray photoelectron spectroscopy (XPS) instrumentation (Physical Electronicz, PHI 5400 and Quantum 2000 ESCA, Eden Prairie, MN, USA) was used in determining the C/O ratio of pelletized BTMP fibres with and without LDH particles before and after oxidative combustion at 350°C. Samples were cut to approx. 0.8 mm×0.5mm pieces in such a way that a clean surface area was revealed from the middle of the pellet. Maximum air exposure was 5 min before the samples were loaded into an ultra-high vacuum (UHV) chamber. A monochromatic Al Kα X-ray source (photon energy 1486.6eV) was used together with an

electron flood gun to neutralize the photoelectric effect generated positive charge on sample surface. X-ray anode was operated at 14.5kV power being 300W (PHI 5400) and 49.0W (Quantum 2000). Take-off angle was 45° and the imaging area was set to 1.5 mm^2 (PHI 5400) and 200 µm (Quantum 2000). Survey-mode photoelectron spectra were acquired with 89.45eV (PHI 5400) and 117.40eV (Quantum 2000) pass-energy and 0.5eV steps. UHV base pressure was held around 5×10^{-9} Torr during the measurements, and reference photoelectron spectra were taken from 100 % cellulose samples before and after measurements to ensure the environment of the UHV chamber remained stable and no sample contamination occurred during the acquisitions.

Results and discussion

Material characterization

Urea hydrolysis is commonly used for homogeneous precipitation of different inorganic metals [28] and provides an easy method to achieve uniform crystalline structures of LDH as confirmed by others [29,30]. Also, in our previous work we noted that pulp fibres from the so called Kraft process can be mineralized with nano-size LDH by urea hydrolysis while in the alternative homogeneous co-precipitation synthesis route the sub-micron and nano-sized particles are generated mainly on pulp fibre surface [27]. By applying both methods in sequence the fibres should be loaded with high number of inorganic nanoparticles.

The weight of Mg^{2+} and Al^{3+} in fibres after the sequential particle synthesis was close to (9.2±0.3)% (w/w), while the amount ratio for Mg^{2+} and Al^{3+} was 1.60±0.05 (Table 1). The absorbed and interlayer water is lost from LDH at approximately 200°C. [31] Water content in LDH depends on the synthesis route. After urea hydrolysis the content, according to thermogravimetry, was close to 14% (w/w) while after homogeneous co-precipitation it was 15% (w/w) [27]. A general formula for the *in situ* synthesised LDH can therefore be written according to Eq. 1. In homogeneous co-precipitation the intercalated carbonate may be substituted to some extent by the precursor anions, in our case by the NO_3^-. In that case the amount of water may also change. Investigation for the substitution extent between NO_3^- and CO_3^{2-} is ongoing. The thermogravimetric analysis that was carried out under air flow from the LDH-lwFF revealed the total non-combustible material content to be (20±1)% (Figure 1). Weight loss patterns were similar to what has been observed with lignin containing fibres by others [32]. Knowing that some (42±2)% of weight from synthesised Mg-Al LDH with carbonate ion is lost during the TG run in the given temperature range, [27] we calculated the initial mineral content in the LDH-lwFF after the *in situ* synthesis route to be approximately (34±2)%. The sudden weight loss and the associated exothermic signal at around 400°C (Figure 1A) were caused by material ignition that occurred repeatedly in repetitious measurements. High amount of LDH particles provided notable reduction in exothermic energy release (Figure 1B) and ignition was suppressed.

$$[Mg_{16}^{2+}Al_{10}^{3+}(OH)_{52}]^{10+}(CO_3^{2-})_5 \cdot 18H_2O \quad (1)$$

Transmission electron microscope revealed that large fraction of nano- and microparticles was unattached onto the fibre wall (Figure 2B). It is well known that the content of carboxylic groups in BTMP is higher than in pulp fibres obtained from the so called Kraft process. After Kraft process the fibres are in practice also free from lignin. The main contributors to the acidity, and therefore to carboxylic content in BTMP, are pectic and uronic acids [33]. The distribution of pectins is known to favour fines over the fibres.[34] On the other hand, at higher pH values (≥ 10), as those in LDH synthesis, the phenolic hydroxyls become acidic as well [35]. SEM imaging revealed large proportions of fibrillary and flake like fines in LDH-lwFF sample (Figure 3). Therefore the factors contributing to particle nucleation and distribution on BTMP fibres were the relatively high surface area and charge to weight ratio of fines along with the high ionic strength that caused the solvent water to flow out of the semi permeable fibre wall, thus shrinking the fibres according to the osmotic pressure difference at the beginning of particle synthesis. Therefore the particles that appear dispersed in TEM images are actually encapsulating the fines. It should be noted that significant number of particles were detected at the lumen side as well (Figure 2B,C). Given that the particles are bound on

Table 1: The ICP-MS results for Mg^{2+} and Al^{3+} content in pulp fibres

Sample	Mg (mg/g)	Al (mg/g)	Mg/Al (n/n)
lwFF	0.07	0.1	-
LDH-lwFF	54±1	37.5±0.7	1.60±0.05

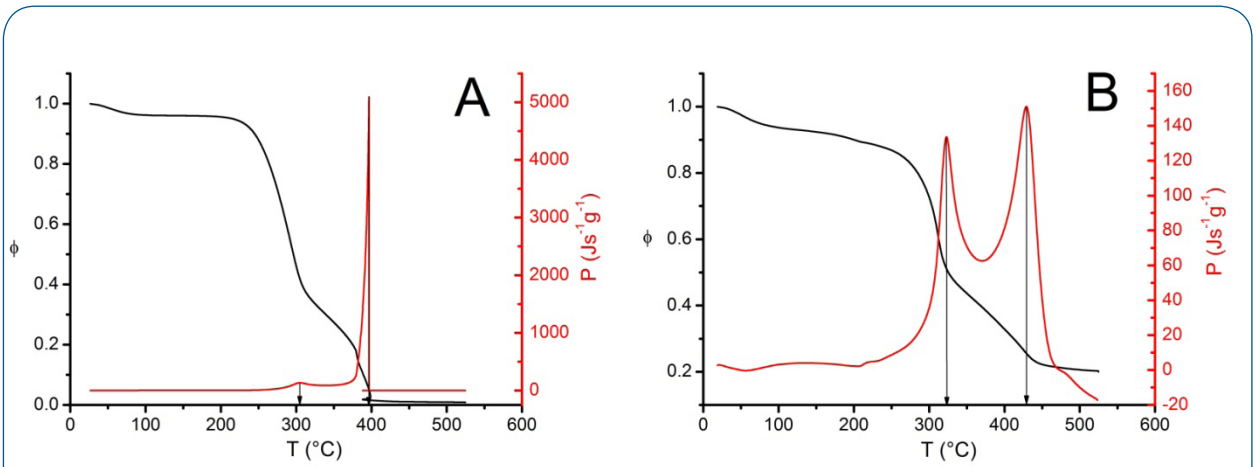

Figure 1: Thermogravimetric analysis for reference lwFF (A) and LDH-lwFF (B). Mass fraction (φ) and energy release (P) are plotted against the temperature

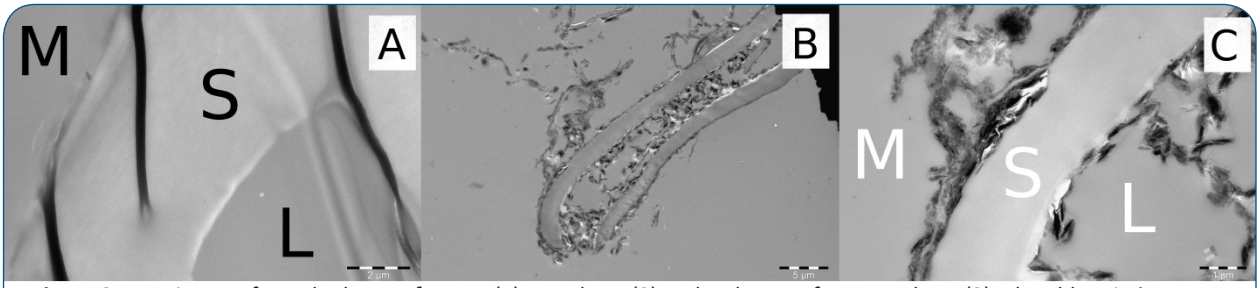

Figure 2: TEM images from the lwFF reference (1), LDH-lwFF (2) and a close up from LDH-lwFF (3). The abbreviations are: M= matrix, S= cell wall and L= lumen

the surface of fibres and fines by electrostatic forces only without the aid of additional polymers often used for enabling e.g. kaolin retention on fibres in paper production, the amount of mineral on fibres and fines is substantial. Sequenced heterogeneous and homogeneous synthesis of LDH at high ionic strength is therefore beneficial in applications where fibre wall should remain intact – and therefore fibres stiffness should not change – but where large weight fraction of inorganics is nevertheless preferred as in flame retardant materials.

SEM images and EDS from lwFF are presented in Figure 3. Only trace amounts of sulphur was detected on the surface layer of reference fibres. Since none was detected in the middle layer, the surfactant must have adsorbed onto the fibres during the dewatering of foam-laid fibre web. In this case the water flow occurs in one direction that makes the foamed bed to behave like a filter for the surfactant. Trace amounts of Na, Ca, Mg, Al and Si were found from reference fibres as well.

The LDH-lwFF retained sulphur both in surface and in middle layers regardless of the place where the spectra were acquired from (Figure 3). Approximation for surface adsorption of surfactant can be done via aluminium to sulphur ratio (Table 2). Surface and middle layers gave similar results for Mg/Al ratio but

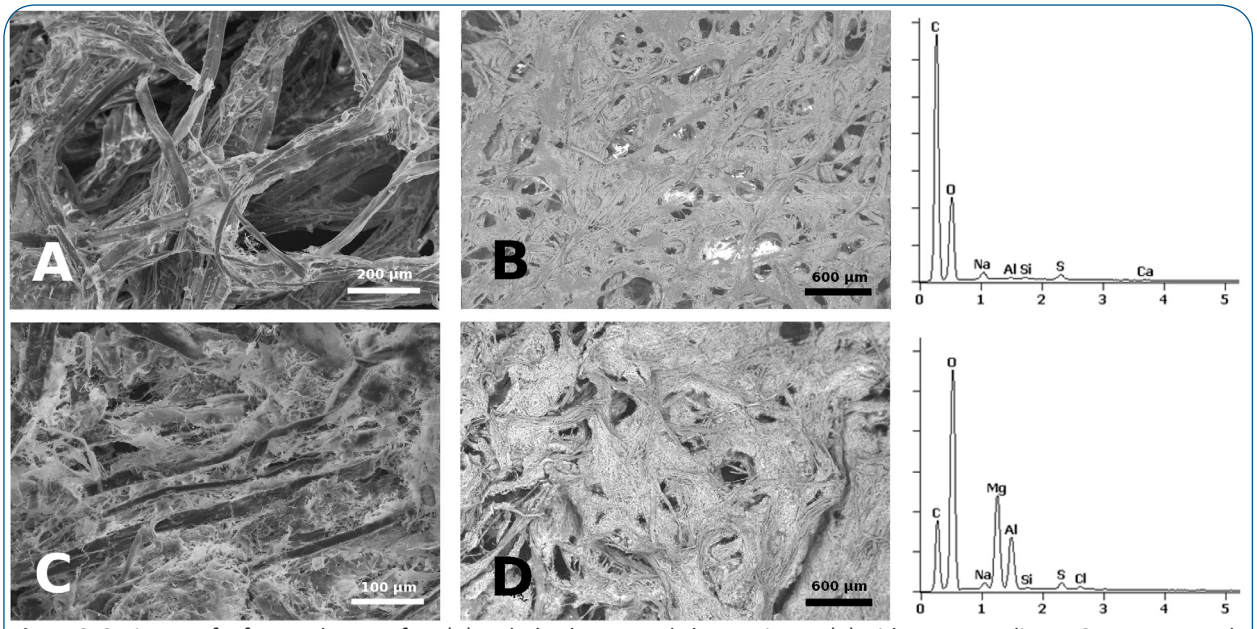

Figure 3: SEI image of reference lwFF surface (A) and a back scattered electron image (B) with corresponding EDS spectrum, and, a SEI image of LDH-lwFF (C) and a back scattered electron image (D) with corresponding EDSspectrum

Table 2: The metal content in LDH-lwFF according to EDS. Data was collected from the foam surface layer, middle layer and from individual fibres in the middle layer. The relative error for each experiment after taking the geometric average from five measurements was 5% or less

Elements	LDH-lwFF		
	Surface	Middle	Fibre
Mg / Al	1.5	1.4	1.6
Al / S	7.9	9.0	7.5

the sulphur content seemed higher on the foam surface. On the other hand, the sulphur content in fibres that contained fines was close to the averaged value found from the LDH-lwFF surface. As mentioned above, significant amount of fines generated during the particle synthesis remained on the surface of the LDH-lwFF (Figure 3C,D). The EDS revealed high concentrations of Mg^{2+} and Al^{3+}. Because the LDH are formed from the hydroxides the oxygen signal has also gone up in relative to carbon. The contrast enhanced images acquired from the back scattered electrons detector show large areas to contain heavier elements than carbon in LDH-lwFF.

A typical IR signal from the LDH structure is the bending vibration of CO_3^{2-} that appears at 1358 cm^{-1} while the stretch vibrations of oxygen–metal bonds are located at lower energies around 779 cm^{-1} and 447 cm^{-1} (Figure 4). These signals were missing in reference lwFF but abundantly present in the LDH-lwFF. All of the findings above verify that large number of LDH particles was associated with fines structures due to their high surface area and high acidic content, and, that the surfactant was

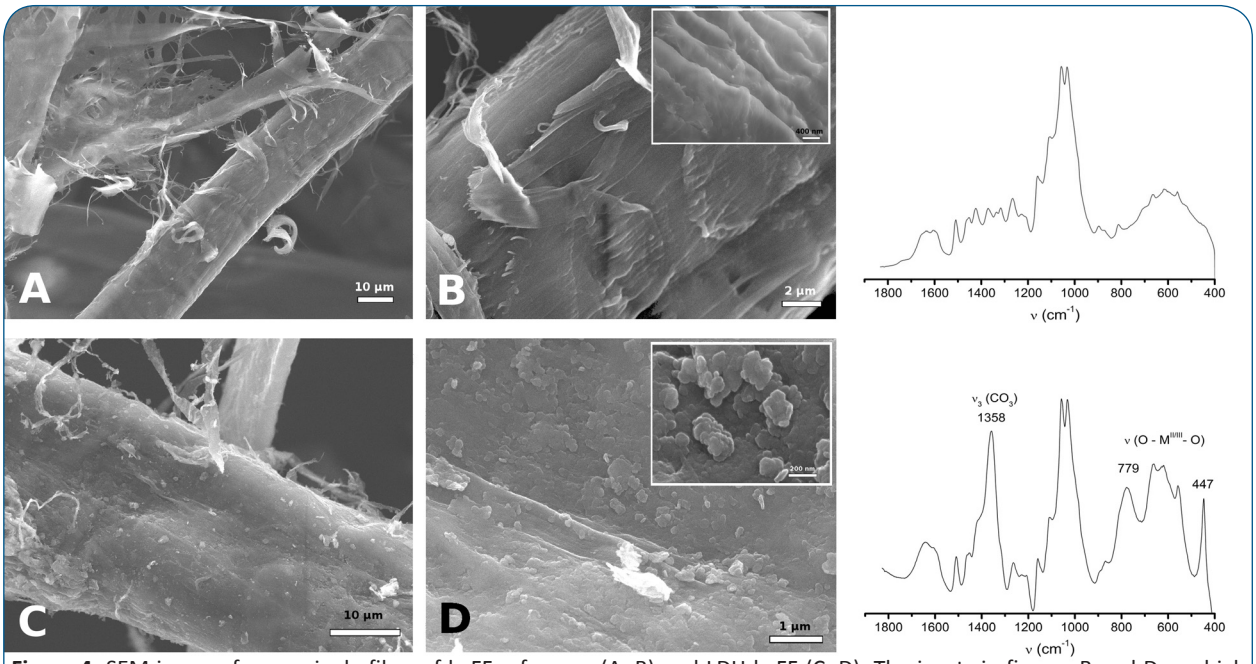

Figure 4: SEM images from a single fibre of lwFF reference (A, B) and LDH-lwFF (C, D). The insets in figures B and D are high magnifications to show the fibre surface features. FTIR spectra from the bulk samples are presented also

effectively filtered off of the solvent phase by LDH.

It was also interesting to note that none of the micron sized LDH particles that the urea hydrolysis typically produce were found from the fibre surface. Only nano-sized particles were observed (Figure 4D). Comparing the TEM images, it seems that larger particles from urea hydrolysis were covered by the smaller ones synthesised via co-precipitation route (Figure 2C).

Combustion behaviour

Experiments that are performed with cone calorimeter are influenced for example by the vertical distance of a sample from the external heat source, applied heat flux, sample holder system and the physical dimensions of the specimen. Applicability of CC in prediction of hazardous fires has been discussed by others [36,37]. In our experiment the distance of the sample surface from the external heat source was 60 mm. This distance is relatively long and may cause the centre of the sample to absorb higher relative irradiance per unit time than the sample edges [36]. However, the tested lwFF were dimensionally unstable under forced burning. The relatively low irradiance (25 $kW \cdot m^{-2}$) was chosen based on that characteristic and was targeted to address the ignition of lwFF. Sample thickness is also an important factor in CC experiments. Foam-laid fibre panels are meant to be applied as a bulk material wherefore the chosen 7.5 mm thickness is within a practical limit. Typically, several such layers are combined to a lamellar structure that is eventually compressed to appropriate density in a suitable mould. Thin samples tend to show higher peak heat release rate (PHRR) values while thick samples burn longer allowing better estimation of flame propagation within the structure. Also, the cut samples were placed on a 20µm thick aluminium tray. Aluminium is a heat conductor and transports irradiated heat away from the sample. The effect of thermal transport is assumed to be small, however, because the wood fibres are good heat insulators, and, because the contact interface area in between the sample and aluminium tray was considerably smaller than the geometrically measured flat surface area of the specimen.

Although CC cannot mimic real fire due to measurement restrictions its importance is in data related to the material behaviour after heat radiation impinges the sample surface. In cone calorimeter the HRR is the most important factor and it is calculated from the flue gas oxygen consumption. Anything that limits oxygen usage upon flaming, such as generation of soot, decarbonation, temperature drop within the material, water evaporation, etc., will affect the observed HRR.[38] The *in situ* synthesised LDH particles on fibres provided reduction in PHRR, CO_2 production rate and smoke yield (Figure 5A,B and Table 3). Tailing in HRR signal predicts that both systems are charring to some extent. The mass loss rate is reduced in LDH-lwFF sample (Figure 5E) indicating slower material volatilization. Narrow HRR profile – rapid combustion – was expected due to the sample thickness. Carbon monoxide yield and production rate increased relative to lwFF reference. Partial oxidation that appeared before the advancing heat release in both samples, also related to CO production and material pyrolysis at the reaction zone front, appeared similar in rate and yield. The production rate of CO in material glowing phase, i.e. after the combustible volatiles have been released but the temperature remains sufficiently high to maintain the material pyrolysis, however, was approx. three times faster in case of LDH-lwFF (Figure 5C,D). Combustion efficiency, yet another important characteristic in CC experimentation, defined as a ratio of total heat evolved (THE) to mass loss change until flame out, was reduced by LDH (Figure 5F).

Some researchers have suggested that materials safety in case of fire can be evaluated and characterized indicatively from CC results by simple calculations based on PHRR, t_{ig} and total energy release [39,40]. For example, in our case, the so called flash over propensity, defined as the ratio of PHRR to t_{ig} drops from initial 22 (high risk) of lwFF to 6 (moderate risk) in LDH-lwFF. Total energy release provided a low risk assessment for both samples. Also, the smoke production subsided within 15s after ignition in case of LDH-lwFF while, for the reference foam,

Table 3: Combustion parameters from CC experiments of five replicate samples. t_{IG} = time to ignition, t_{FO} = time to flame out, PHRR = peak heat release rate, ψ_{CO} and ψ_{CO2} = CO and CO_2 production yields, v_{CO} and v_{CO2} = maximum CO and CO_2 emission rates, E = total energy release, τ = total smoke release

Sample	t_{IG} (s)	t_{FO} (s)	PHRR (kW/m²) [Gap_{ig} / s][1]	ψ_{CO} (kg/kg) [ψ / %][2]	ψ_{CO2} (kg/kg) [ψ / %][2]	v_{CO} (mg/s)		v_{CO2} (mg/s)		E (MJ/m²)	τ(m²)
						1.peak	2.peak	1.peak	2.peak		
lwFF	8±1	24±2	177±6 [14]	0.058±0.004 [2.1]	2.7±0.3 [97.9]	1.8±0.2	2.1±0.2	127±7	133±7	3.7±0.2	0.17±0.02
LDH-lwFF	12±1	34±3	68±10 [20]	0.18±0.03 [6.5]	2.6±0.2 [93.5]	2±1	4.6±0.3	40±20	51±7	2.1±0.1	0.04±0.03

[1]Gap_{ig} in brackets refers to the average elapsed time in seconds from the material ignition to the peak value

[2]The fraction (ψ) of the volatile gas from the total gas production is presented in brackets

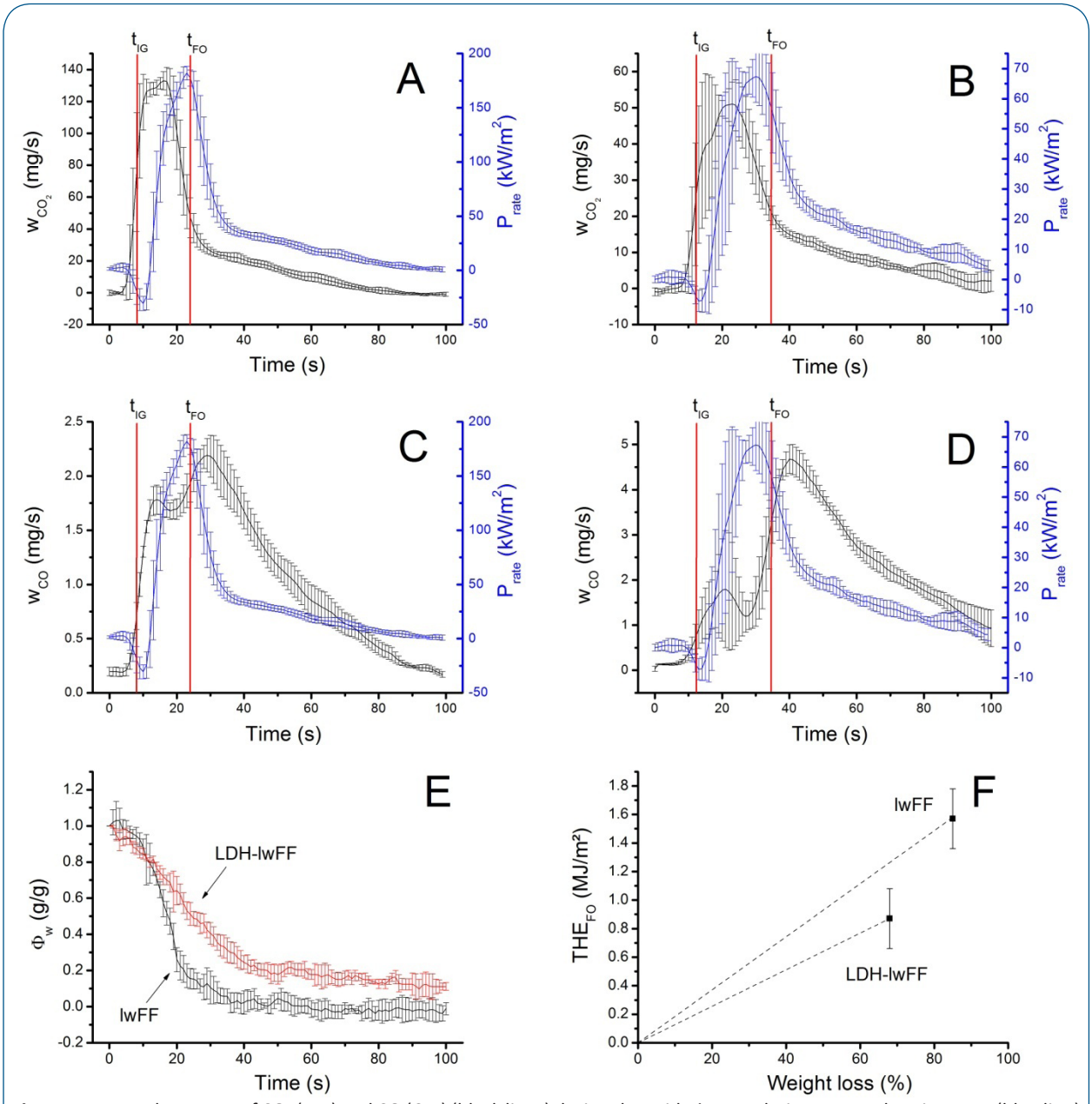

Figure 5: Mass release rate of CO_2 (A,B) and CO (C,D) (black lines) during the oxidative pyrolysis compared against HRR (blue line) in lwFF reference (A,C) and LDH-lwFF (B,D), and, data from mass fraction extent (E) and combustion efficiency (F) are presented. Time to ignition (t_{IG}) and time to flame out (t_{FO}) are marked with red vertical lines

it took nearly 22s. Amount of soot was about four times greater in reference lwFF sample (Table 3). The mineral containing foam will therefore produce less fine particulates upon fire. In comparison, e.g. the ammonium polyphosphate treated plywood released significantly higher amounts of smoke than the reference sample while the PHRR values and the relative amounts of CO formation were similar to our experiments [41]. It was interesting to note that the flame subsided slower in LDH-lwFF; albeit it did not develop as it did for the reference lwFF. The nano-sized LDH particles act as heat barrier and reduce the liberation of burning volatiles. An example of material morphology after combustion is given in Figure 6. Carbonized organic substances are seen on lwFF (Figure 6A) while particles that resemble features of fibres are seen in LDH-lwFF (Figure 6B).

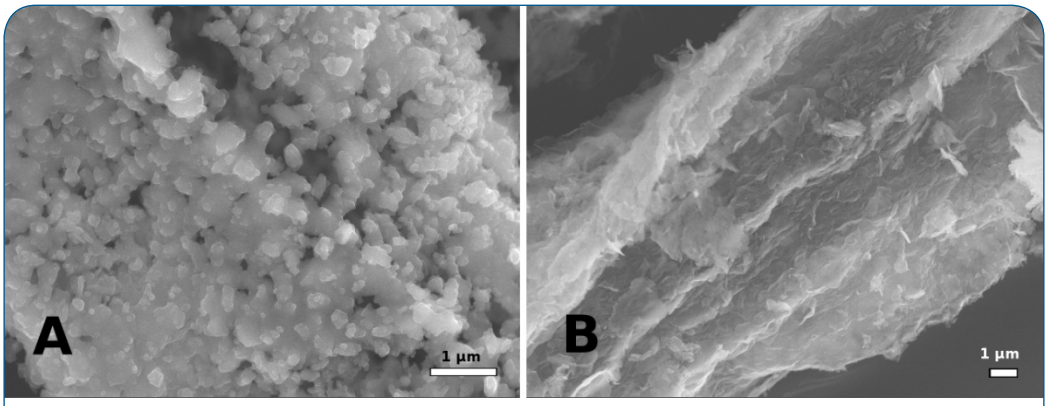

Figure 6: SEM close up images from the large residues of reference lwFF (A) and LDH-lwFF (B) after oxidative pyrolysis in cone calorimeter

composition and chemical structure of materials surfaces. In our study the carbon content on materials surface was found to be relatively high after the combustion (Table 4). The LDH contain

The combustion of volatiles in CC was rapid and the glowing stage was also subsiding within 90s after material ignition. It is known that heat transfer from the external heat flux and from the flame in CC is in the same order of magnitude. It is therefore assumed that dehydroxylation and loss of carbonate in a form of water and CO_2, and, volatization of the free and crystalline water, comprising 15% from total weight of LDH, leading to rocksalt structure, occur during the combustion phase.

To find out how the ratio of C to O changed during the pyrolytic phase in CC, i.e. at the beginning of the combustion process, X-ray photoelectron spectroscopy was utilized before and after the process. Photoelectron spectroscopy is highly surface sensitive analysis technique penetrating some tens of nanometres into the material and it is widely used in investigation of elementary carbon only in a form of inorganic carbonate. Considering the chemical formula for LDH (see Eq. 1) we can conclude that the relative amount of carbon from organic material has obscured

Table 4: The elemental surface composition of C, O, Mg and Al from the pelletized lwFF and LDH-lwFF that was also oxidatively pyrolysed in cone calorimeter experiment (LDH-lwFF^{cc}). The values are given in atomic weight per centile. The relative change (v) in % for C1s and O1s signals and C/O ratio after 2 min of controlled burning sequence is also given

Sample	C1s	O1s	Mg2s	Al2p	C/O	v(C1s) 1/min	v(O1s) 1/min	v(C/O) 1/min
lwFF	66±1	35±1	-	-	1.9±0.2	3	-3	0.9
LDH-lwFF	33±1	51±1	10±2	5±2	0.65±0.07	7	-4.5	0.6
LDH-lwFF ^{cc}	18±2	58±2	15±1	9±1	0.31±0.05	-	-	-

the detection of photoelectrons originated from Mg^{2+} and Al^{3+}. This organic material includes possibly xylan and other hemicelluloses that are typically redeposited on pulp fibres during the alkaline processes at elevated temperatures, such as those in LDH synthesis. Even though sample transferring via air has also caused some additional C and O concentration on the surface, the effect is assumed to be small and systematic for all samples. After oxidative pyrolysis precursor metals were detected in similar proportions by XPS compared to the EDS and ICP-MS results from the bulk material (cf. Table 1 and 2). The relative amount of carbon remained still high, which can be explained only by charred organic material on the surface of nano-sized LDH.

In case of lwFF abrupt changes in carbon and oxygen contents were detected depending on the duration of the controlled burning at 350°C (Figure 7). The LDH-lwFF sample provided more gradual change for both elements. The rate of change of C to O ratio after initiation at 2 min was 0.9 min^{-1} for lwFF and 0.6 min^{-1} for LDH-lwFF (Table 4). However, comparing C1s and O1s values detected in both samples the relative amount of carbon increases faster on particle surface. Mineral content alone cannot explain these changes. It appears therefore that the heat transfer is restricted in the presence of nano-sized LDH due to the known transformation processes taking place in the mineral. Temperature drop is expected across the mineral layer on the fibre surface that

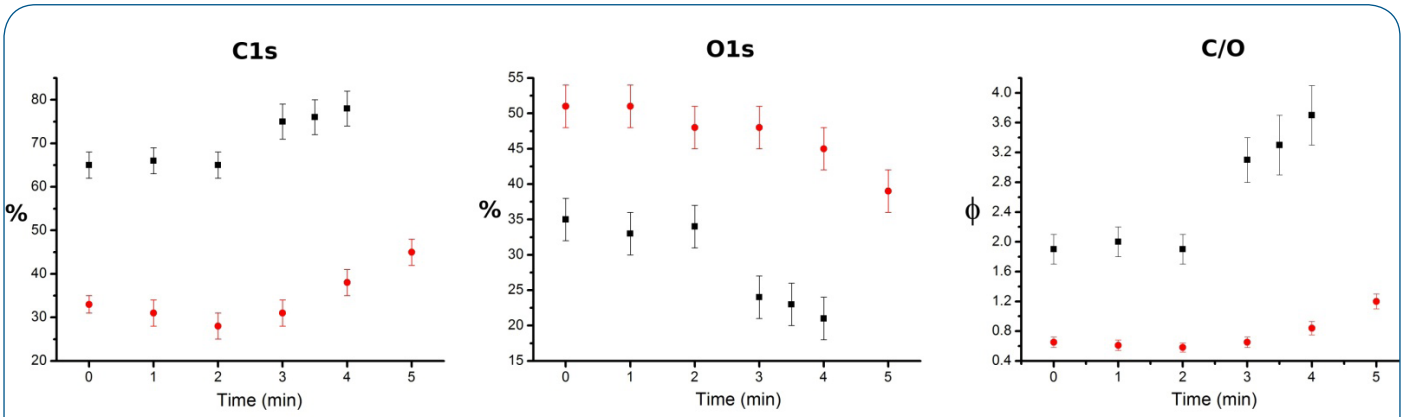

Figure 7: XPS results for C1s and O1s contents in % from pelletized lwFF reference (■) and LDH-lwFF (●) after oxidative pyrolysis at 350°C

leads to inefficient oxidation of organic material. However the pyrolysis on particle surface appears relatively rapid. The effect of controlled burning at 280°C and 340°C in confined space in a muffle oven that allow only convection of gaseous products are shown in Figure 8. Oxidation of BTMP fibres in presence of LDH particles enabled similar alterations in the chemical composition that were found with Kraft fibres in our earlier study [27]. The unconjugated stretch vibration of carboxylic acids at 1715 cm^{-1} [42] increases significantly in lwFF at 340°C (Figure 8B). In LDH-lwFF the oxidation to acids is almost non-existent (Figure

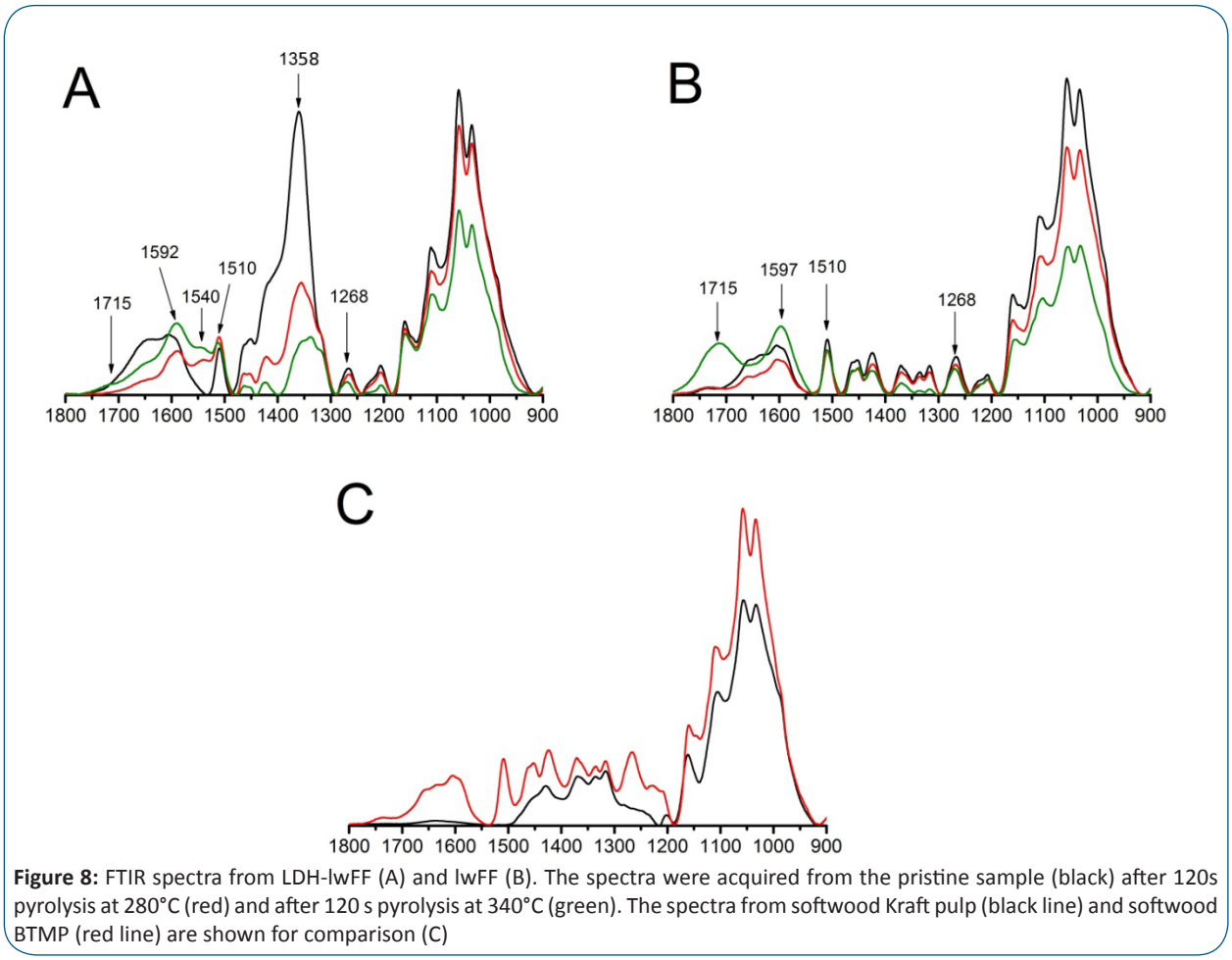

Figure 8: FTIR spectra from LDH-lwFF (A) and lwFF (B). The spectra were acquired from the pristine sample (black) after 120s pyrolysis at 280°C (red) and after 120 s pyrolysis at 340°C (green). The spectra from softwood Kraft pulp (black line) and softwood BTMP (red line) are shown for comparison (C)

8A). It is worth noting that the skeletal vibration from phenolic units of lignin at 1510 cm^{-1} does not show major changes in relative strength at these temperatures in the given time frame. Changes in the regions that arise primarily from vibrations of carbohydrates, viz. 950 - 1150 cm^{-1} and 1300 - 1425 cm^{-1} are, due to thermodynamic considerations, relatively intense in comparison to those that arise from the aromatic units. Oxidation is therefore directed to the carbohydrates over the phenolic moieties. Also, the strong absorption from the carbonate (see above Figure 4) precludes the possibility to determine changes in lignin in that range in case of LDH-lwFF. Furthermore the lwFF reference does not have absorption band at 1540 cm^{-1}. This band arises from the splitting of carbonate vibration during the pyrolysis as explained elsewhere [27]. Partial oxidation contributes to the formation of diones and ketones that are observed in 1592 - 1597 cm^{-1} in both samples. It was interesting to note that the absorption

bands arising from the ring vibration of guaiacyl lignin at 1268 cm^{-1} [42] had relatively low absorption intensity in LDH-lwFF sample. Similar reduction in absorption has been observed e.g. during the Kraft cooking of softwood pulp fibres [43]. The *in situ* synthesis of LDH with thermomechanical softwood pulp fibres must therefore affect similarly to the lignin structure as does the conventional Kraft cooking process. The common nominator here is the alkalinity of the medium.

Examples from the ignition, flame spread and incineration of foam-laid samples by HSvid observations are shown in Figures 9 and 10. The advancing flame front is preceded by materials dimensional changes that were attributed to loss of easily volatized compounds, such as water, and, the fibre collapse. Dimensional changes in lwFF seemed to occur everywhere in the area of imaging approximately at the same time. In LDH-lwFF the dimensional changes were subtle. The flame spread and incineration, on the other hand, were conducted from fibre to fibre. Once the flame was initiated by the heated resistive wire the material incinerated from that point onward. It was noted above that majority of CO_2 is released after ignition. During the oxidative pyrolysis of LDH-lwFF the flame spread was observed as an advancing glow, yet the incineration was practically completely dampened by the

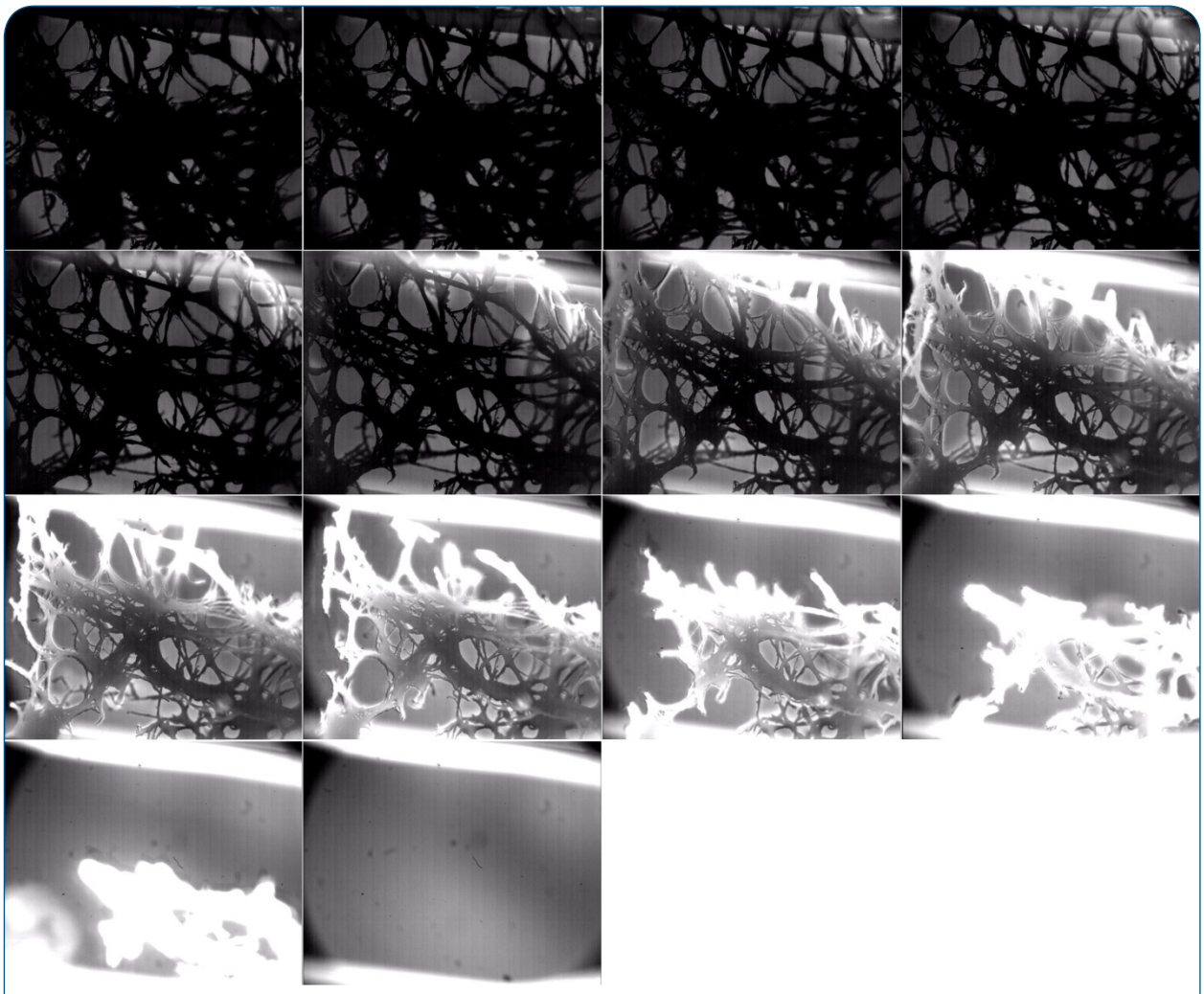

Figure 9: Image collage from the lwFF reference. Each frame was taken in 50 ms intervals. The burning proceeds from the top to bottom. The resistive wire that changes its brightness in each image is 250 µm in thickness. The images were acquired with ISO 400 sensitivity and 1.4 ms exposure time

particles on the fibre surface. Since the exothermic reactions observed in TG suggest that both samples carry similar energies in form of combustible material, provided the temperature ramp is reasonably slow, the fast pyrolytic temperature change due to external heat flux and flaming zone must be used up by LDH. Therefore the buffering effect comes in the form of shielding the material from external heat source.

Conclusion

We envisage that nanoengineering of hybrid materials can provide a sustainable method to inhibit flammability in wood derived products in general. The precursors for LDH particles particularly are cheap and the nanoparticles are easy to manufacture from aqueous solution, which are all practical advantages for the industrial process. Also, for example, in comparison to halogen-based flame retardants, the LDH that is synthesised from Mg^{2+} and Al^{3+} precursors has a benefit from low level of toxicity and environmental impact that are both important factors from the end user perspective. LDH seem to offer benefit over polyphosphates in that the generation of smoke is reduced, which reduces inhalation of small particulates in case of fire. It appears that the impinging heat is shielded by the LDH particles and the effect is amplified by char formation as the organic material is oxidized to a lesser degree in the same time

Figure 10: Image collage from the LDH-lwFF. Each frame was taken in 50 ms intervals. The burning proceeds from the upper left hand corner towards the lower right hand corner. The resistive wire that changes its brightness in each image is 250 µm in thickness. The images were acquired with ISO 400 sensitivity and 1.4 ms exposure time

frame in comparison to the reference material. The conclusions derived from this study can be summarized as follows.

- Utilizing nanoengineering through sequenced *in situ* particle synthesis via urea hydrolysis and homogeneous co-precipitation results high mineral content (34±2)% on fibre surfaces.
- Fine structures, such as flakes and fibrils, are prone for LDH nucleation and favoured over fibres.
- LDH provide a relatively dense structure enveloping the fibres.
- Synthesis of LDH at alkaline conditions liberates organic material from the mechanically pulped fibres, and, provides re-deposition of these substances onto the particle surface.
- The flammability, production of soot and CO_2 production rate during the oxidative pyrolysis were significantly reduced by carbonate containing nano- and micron sized LDH particles.
- The *in situ* synthesised LDH particles retarded the rate of pyrolysis of biofibres and appear to restrict liberation of volatiles after ignition thus slowing down the flame propagation.
- Charring was initiated at the interphase of nano-sized LDH and organic material that in turn amplifies the flame retardant effect. However, partial oxidation on particle surface appears relatively rapid.

Acknowledgements

We would like to thank UPM-Kymmene Rauma mill for providing the pulp for this study. We also would like to acknowledge all the laboratory personnel at Åbo Akademi University who assisted with the instrumentation. Carl Lange carried out the study, as part of his Ph.D. project, and was responsible for all parts of the research project, including writing the manuscript. Dr. Jan-Erik Eriksson operated the conical calorimeter with the author, Paul Ek operated the ICP-MS instrument and Jani Lehmonen was responsible for preparing the foam-laid fibre panels. The help in TEM instrumentation by Markus Peurla and Jenni Laine is acknowledged. XPS study was mainly performed by Marjukka Tuominen. Pedro Fardim was responsible for overall supervision.

References

1. Bryant FL. Distended fibrous material and Process of producing the same. United States Patent: US1740280A. 1929.
2. Gatward APJ, Radvan B. Method of producing a thixotropic liquid suspending medium particularly for the forming of non-woven fibrous webs. United Kingdom Patent: GB1129757(A). 1968.
3. Wilcox FS. Process of dispersing fibrous material in a foam and resulting product. United States Patent: US3007840A. 1961.
4. Smith, Malcolm K. Method of producing non-woven fibrous material. United States Patent: US3947315A. 1976.
5. Radvan B,Gatward APJ. The Formation of Wet-Laid Webs by a Foaming Process. TAPPI Journal. 1972; 55(5):748–751.
6. Smith MK,Punton VW,Rixson AG. The St Process and Properties of Paper Formed by a Foaming Process. TAPPI Journal. 1974; 57(1):107–111.
7. Lappalainen T, Lehmonen J. Determinations of bubble size distribution of foam-fibre mixture using circular Hough transform. Nordic Pulp & Paper Research Journal. 2012; 27(5):930–939.
8. Madani A,Zeinoddini S,Varahmi S, Turnbull H,Phillion AB, Olson JA,et al. Ultra-lightweight paper foams: proprocess and properties. Cellulose. 2014; 21:2023–2031.doi:10.1007/s10570-014-0197-3.
9. Rantanen J,Dimic-Misic K, Pirttiniemi J, Kuosmanen P,Maloney TC. Forming and Dewatering of a Microfibrillated Cellulose Composite Paper. BioResources. 2015; 10(2):3492–3506.
10. Salas C,Nypelö T, Rodriguez-Abreu C, Carrillo C, Rojas OJ. Nanocellulose properties and applications in colloids and interfaces. Current Opinion in Colloid & Interface Science. 2014; 19(5):383–396.doi:10.1016/j.cocis.2014.10.003.
11. Isogai Akira. Wood nanocelluloses: fundamentals and applications as new bio-based nanomaterials. Journal of Wood Science. 2013; 59(6):449–459.doi: 10.1007/s10086-013-1365-z.
12. Cervin NT,Andersson L, Ng JBS, Olin P, BergströmL,Wågberg L. Lightweight and Strong Cellulose Materials Made from Aqueous Foams Stabilized by Nanofibrillated Cellulose. Biomacromolecules. 2013; 14(2):503–511.doi: 10.1021/bm301755u.
13. Lorenz TJ,Polat O,Trokhan PD, Phan D. Process for making a fibrous structure comprising cellulosic and synthetic fibers. United States Patent: US7645359B2. 2010.
14. Blomqvist R,Kostamo H, Laine E,Rokman K. Method and apparatus for foam forming. United States Patent: US7416636B2. 2008.
15. Dwiggins JH, Bhat DM. Foam forming method and apparatus. United States Patent: US6500302B2. 2002.
16. Saito I,Onuki A,Seto H. Indoor organophosphate and polybrominated flame retardants in Tokyo. Indoor Air. 2007; 17(1):28–36.
17. Oliveri AN, Bailey JM, Levin ED. Developmental exposure to organophosphate flame retardants causes behavioral effects in larval and adult zebrafish. NeurotoxicolTeratol. 2015.doi: 10.1016/j.ntt.2015.08.008.
18. Stanimirova T, Hibino T,Balek V. Thermal behavior of Mg-Al-CO_3 layered double hydroxide characterized by emanation thermal analysis. Journal of Thermal Analysis and Calorimetry. 2006; 84(2):473–478.doi: 10.1007/s10973-005-7283-6.
19. Stanimirova T,Piperov N,Petrova N, Kirov G. Thermal evolution of Mg-Al-CO_3hydrotalcites. Clay Minerals. 2004; 39:177–191.doi: 10.1180/0009855043920129.
20. Hibino T, Yamashita Y, Kosuge K, Tsunashima A. Decarbonation behavior of Ma-Al-CO_3 Hydrotalcite-like compounds during heat treatment. Clays and Clay Minerals. 1995; 43(4):427–432.doi: 10.1346/CCMN.1995.0430405.
21. Gao Y, Wu J, Wang Q,Wilkie CA, O´Hare D. Flame retardant polymer/layered double hydroxide nanocomposites. Journal of Materials Chemistry. 2014; 2:10996–11016.doi: 10.1039/C4TA01030B.
22. Wang X, Zhang Q. Effect of hydrotalcite on the thermal stability, mechanical properties, rheology and flame retardance of poly(vinyl chloride). Polymer International. 2004; 53(6):698–707.doi: 10.1002/pi.1482.
23. Nyambo C,Songtipya P, Manias E, Jimenez-Gasco MM,Wilkie CA. Effect of MgAl-layered double hydroxide exchanged with linear alkyl carboxylates on fire-retardancy of PMMA and PS. Journal of Materials Chemistry. 2008; 18:4827–4838.doi:10.1039/B806531D.
24. Xu S, Zhang L, Lin Y, Li R, Zhang F. Layered double hydroxides used as flame retardant for engineering plastic acrylonitrile–butadiene–styrene (ABS). Journal of Physics and Chemistry of Solids. 2012; 73(12):1514–1517.doi:10.1016/j.jpcs.2012.04.011.
25. Wang S, Huang J, Chen F. Study on Mg-Al hydrotalcites in flame-retardant paper preparation. BioResources. 2012; 7(1):997–1007.
26. Li YC,Mannen S, Cain AC,Grunlan J. Layer-by-layer assembly of layered double hydroxides on cotton fabric for anti-flammability. Conference Proceedings241st ACS National Meeting & Exposition; Anaheim, CA, USA. 2011. p. 27-31.
27. Lange CE,Lastusaari M, Reza M,Latifi SK,Kallio P, Fardim P. In situ Hybridization of Pulp Fibres Using Mg-Al Layered Double Hydroxides. Fibers. 2015; 3(2):103–133.doi:10.3390/fib3020103.
28. Harris DC. Quantitative Chemical Analysis. 6th ed.NY: WH Freeman and Company; 2002. 684 – 686 p.
29. Costantino U,Marmottini F,Nocchetti M,Vivani R. New Synthetic Routes to Hydrotalcite-Like Compounds 2 Characterisation and Properties of the Obtained Materials. European Journal of Inorganic Chemistry. 1998; 1998(10):1439–1446.doi: 10.1002/(SICI)1099-0682(199810)1998:10<1439::AID-EJIC1439>3.0.CO;2-1.
30. Ogawa M,Kaiho H. Homogeneous Precipitation of Uniform Hydrotalcite Particles. Langmuir. 2002; 18(11):4240–4242.doi: 10.1021/la0117045.
31. Theiss FL,Ayoko GA, Frost RL. Thermogravimetric analysis of selected layaerd double hydroxides. Journal of Thermal Analysis and Calorimetry. 2013; 112(2):649–657.doi: 10.1007/s10973-012-2584-z.
32. Xiao B, Sun XF, Sun, RunCang. Chemical, structural, and thermal Characterization of alkali-soluble lignins and hemicelluloses, and cellulose from maize stems, rye straw, and rice straw. Polymer Degradation and Stability. 2001; 74(2):307–319.doi: 10.1016/S0141-3910(01)00163-X.
33. Pranovich AV, Sundberg KE, Holmbom BR. Chemical Changes in Thermomechanical Pulp at Alkaline Conditions. Journal of Wood Chemistry and Technology. 2003; 23:89–112.doi: 10.1081/WCT-120018617.
34. Sundberg A, Pranovich A,Holmbom B. Distribution of anionic groups in TMP suspensions. Journal of Wood Chemistry and Technology. 2000; 20(1):71–92.doi: 10.1080/02773810009349625.
35. Kleen M,Kangas H, Laine C. Chemical characterization of mechanical pulp fines and fiber surface layers. Nordic Pulp & Paper Research Journal. 2003; 18(4):361–368.doi: 10.3183/NPPRJ-2003-18-04-p361-368.

36. KuangChung T, Drysdale D. Using cone calorimeter data for the prediction of fire hazard. Fire Safety Journal. 2002; 37(7):697–706. doi:10.1016/S0379-7112(02)00024-3.

37. Schartel B, Hull TR. Development of fire-retarded materials – Interpretation of cone calorimeter data. Fire and Materials. 2007; 31(5):327–354.doi: 10.1002/fam.949.

38. Schartel B,Bartholomai M, Knoll U. Some comments on the use of cone calorimeter data. Polymer Degradation and Stability. 2005; 88(3):540–547.doi:10.1016/j.polymdegradstab.2004.12.016.

39. Petrella RV. The assessment of full-scale fire hazards from cone calorimeter data. Journal of Fire Science. 1992; 12(1):14–43.doi: 10.1177/073490419401200102.

40. Xu Q,Zachar M,Majlingová A,Jin C, Jiang Y. Evaluation of plywood fire behaviour by ISO tests. European Journal of Environmental and Safety Sciences. 2013; 1(1):1–7.

41. Wang M, Wang X, Li L, Ji H. Fire Performance of Plywood Treated with Ammonium Polyphosphate and 4A Zeolite. BioResources. 2014; 9(3):4934 – 4945.

42. Pandey KK. A study of chemical structure of soft and hardwood and wood polymers by FTIR spectroscopy. Journal of Applied Polymeric Science. 1999; 71(12):1969–1975.doi:10.1002/(SICI)1097-4628(19990321)71:12<1969::AID-APP6>3.0.CO;2-D.

43. DerkachevaO,Sukhov D. Investigation of Lignins by FTIR Spectroscopy. Macromolecular Symposia. 2008; 265(1):61–68.doi: 10.1002/masy.200850507.